



Spherical Thermal Counterflow of He II

Zhuolin Xie¹ · Yunhu Huang¹ · Filip Novotný¹ · Šimon Midlik¹ · David Schmoranzer¹ · Ladislav Skrbek¹

Received: 30 September 2021 / Accepted: 23 January 2022 / Published online: 23 February 2022
© The Author(s), under exclusive licence to Springer Science+Business Media, LLC, part of Springer Nature 2022

Abstract

Past investigations of thermal counterflow in He II were mostly conducted in pipes/channels of constant cross-sections, which are often unduly influenced by the presence of walls. We devise and carry out an experiment using a spherically symmetric setup to study unbounded counterflow in order to gain better understanding of interactions between quantized vortices and counterflow; the preliminary analysis shows that this method is viable.

Keywords Superfluid · Counterflow · Vortex · Spherical

1 Heat transport in superfluid ⁴He

Heat transport in superfluid ⁴He (He II) differs from that in classical viscous fluids in that He II at $T \gtrsim 1$ K can be described as a mixture of two components, the superfluid component and the normal one; the total density is the sum of the two component densities $\rho = \rho_s + \rho_n$ [1]. In the past, thermal counterflow of He II had frequently been studied in pipes and channels of constant cross-sections [2–5, 10], typically by applying a heat flux \dot{q} to the dead end of the channel with the other end open to the helium bath.

For small \dot{q} , the flow of the normal fluid is laminar, and there are no quantized vortices in the potential flow of the superfluid component except, in practice, of few remnant vortices due to surface roughness of the channel walls. The normal and superfluid velocity fields are nearly independent, and a constant temperature gradient along the channel is established. Upon increasing \dot{q} thermal counterflow becomes turbulent. In some cases, a tangle of quantized vortex lines becomes generated in the superfluid while the normal fluid remains laminar, forming so-called

✉ Yunhu Huang
yunhu.huang@gmail.com

¹ Faculty of Mathematics and Physics, Charles University, Ke Karlovu 3, Prague 121 16, Czech Republic

TI state of counterflow turbulence [6]. Further increase in heat flux causes the flow to enter the TII state,¹ where both components are turbulent [7, 8]. The presence of the ångström-sized vortex lines couples the normal and superfluid velocity fields by an effective mutual friction force \mathbf{F}_{ns} arising from phonons and rotons scattering off the vortices. Each vortex carries one quantum of circulation $\kappa = h/m_4 \approx 9.97 \times 10^{-8} \text{ m}^2/\text{s}$, where h is the Planck's constant, and m_4 denotes the mass of a ^4He atom [9].

Since the pioneering work of Vinen [2–5], many experimental, theoretical and numerical studies followed. Despite these efforts, many aspects of counterflow turbulence are still not well understood. One reason for the difficulty is that, due to its quantum nature, turbulent thermal counterflow of He II is more complex than classical viscous fluid flow in pipe or channels [10], and various aspects of bulk counterflow and the influence of channel walls are generally very difficult to disentangle.

A possibility to overcome this obstacle is to study unbounded thermal counterflow, thus eliminating the influence of walls. The main idea for the present work follows the first theoretical and numerical study of spherically symmetric counterflow by Varga [11], the subsequent work of Inui and Tsubota [12], as well as the 2D cylindrically symmetric studies of the Newcastle group [13, 14]. We expect the spherical symmetry to confine the direction of counterflow, and consequently of the vortex line density gradient, to be essentially in the radial direction, such that we may avoid the complications arising near boundaries. Here we report the design and working progress of an experiment studying turbulent 3D thermal counterflow of He II in a spherical cell, generated by a small heater and probed by second sound attenuation [15]. Additionally, we discuss our companion experiment where the temperature gradient in 3D counterflow [16] is directly measured using sensitive thermometry.

2 Spherical counterflow

Heat transport in He II follows the empirical relationship $\nabla T = -f(T)\dot{q}^{3,4}$, where $f(T)$ can be viewed as a generalized conductivity [17, 18]. This agrees² with recent measurements performed directly in the bulk liquid for turbulent thermal counterflow in a channel of rectangular cross-section of 7 mm side [16]. Macroscopically, temperature gradient ∇T and vortex line density L are related by Hall-Vinen-Bekarevich-Khalatnikov (HVBK) equations and described by [16, 19]

$$\rho_n \frac{D\mathbf{u}_n}{Dt} = -\frac{\rho_n}{\rho} \nabla p + \eta_n \Delta \mathbf{u}_n - \rho_s \sigma \nabla T + \mathbf{F}_{\text{ns}}, \quad (1a)$$

¹ Additionally, in rectangular channels of high (1:10) aspect ratio with the small dimension less than 100 μm , only one transition has been observed, denoted by Tough as T III [6].

² Except within a thin boundary layer adjacent to the heater, physical origin of which is not yet fully understood [16]

$$\rho_s \frac{D\mathbf{u}_s}{Dt} = -\frac{\rho_s}{\rho} \nabla p + \rho_s \sigma \nabla T - \mathbf{F}_{ns}, \quad (1b)$$

where $D\mathbf{u}/Dt \equiv \partial\mathbf{u}/\partial t + (\mathbf{u}\nabla)\mathbf{u}$, and p , σ , η_n and \mathbf{F}_{ns} are, respectively, the pressure, the specific entropy, the normal fluid dynamic viscosity and the mutual friction force. The latter can be written in a simplified form as [9]

$$\mathbf{F}_{ns} = -\alpha\kappa\rho_s L(\mathbf{u}_n - \mathbf{u}_s), \quad (2)$$

where α is the tabulated dissipative mutual friction parameter [20]. The vortex line density is related to counterflow velocity u_{ns} by

$$L = \gamma^2(u_{ns} - u_c)^2 \approx \gamma^2 u_{ns}^2, \quad (3)$$

where γ is a temperature dependent parameter known within the accuracy of about 20%, while u_c is the critical velocity typically of the order of 1 mm/s.

For spherically symmetric heat flow, Eq. 1 reduce to the 1D case

$$\rho\sigma \frac{\partial T}{\partial r} = -\frac{\rho_n}{2} \frac{\partial}{\partial r} \left[u_n^2 \left(1 - \frac{\rho_n^2}{\rho_s^2} \right) \right] + \eta_n \left(\frac{1}{r^2} \frac{\partial}{\partial r} r^2 \frac{\partial u_n}{\partial r} - \frac{2u_n}{r^2} \right) - \alpha\kappa\gamma^2 \frac{\rho^4}{\rho_s^3} u_n^3. \quad (4)$$

At a distance r from the center, in the steady-state, the heat supply \dot{Q} is carried away by the normal fluid alone: $\dot{Q} = 4\pi r^2 \rho\sigma T u_n$, which, when substituted into Eq. 4, enables us to numerically calculate the temperature gradient.

It is instructive, however, to examine the approximate analytical solution. Assuming that the first two terms on the right-hand side of Eq. 4 are typically negligible (the validity of which can be corroborated by the result of this very calculation) and that the resulting temperature gradient is small, we obtain

$$T(r) = \frac{\alpha\kappa\gamma^2}{5\sigma^4\rho_s^3} \left(\frac{\dot{Q}}{4\pi T} \right)^3 \frac{1}{r^5} + T_0, \quad (5)$$

where T_0 is the bath temperature at infinity. This approximation is sufficiently accurate when compared to the result of full numerical calculation of Eq. 4 under our experimental conditions, i.e., when \dot{Q} is of the order of 100 mW and the distance r varies from millimeters to centimeters.

3 Temperature profile measurement

We separately conducted a complementary experiment to directly measure the temperature distribution surrounding the spherical heater. The setup is shown in Fig. 1. The main body is a hollow frame, 3D printed using the copper-doped PLA filament. The spherical heater ~ 2 mm in diameter is made of a surface-mount device resistor encased in Stycast and silver epoxy, suspended from a thin tube which houses the heater leads. The upper end of the tube is connected to the driving shaft of a precision linear motor, thus the heater assembly can be moved in the vertical direction

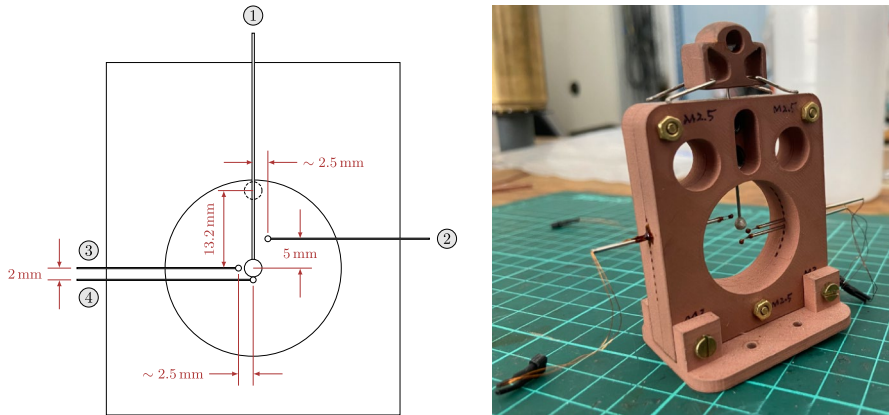


Fig. 1 Schematic diagram and photograph of the temperature profile measurement setup. Labels in the diagram denote the connection to the linear motor (1); and to the TTRG thermometers (2–4) (Color figure online)

freely within its range of travel ~ 13 mm. Three TTRG thermometers [21–23] are ~ 0.5 mm in size and are mounted on the sides of the frame such that when the heater travels along its vertical path, each thermometer will be as close as ~ 0.1 mm to the heater surface.

The entire setup is then put into the helium bath with its temperature controlled using a pumping unit consisting of a Roots pump and a mechanical backing pump. We apply power ranging from 200 mW to 660 mW to the heater at temperatures from 1.25 K to 2 K. For each power and temperature, the heater was set at multiple vertical positions and readings of all three thermometers were recorded, all automated by a custom LabView program. Thus, we obtain the relation between the temperature change at each thermometer and its distance from the heater, from where we can deduce the temperature profile around a stationary heater.

Preliminary analysis (e.g., Fig. 2) shows that the measured temperature profiles agree with the formulation given in the previous section. In particular, if $r \gtrsim 2$ mm or the heater power is below $\lesssim 200$ mW, Eq. 5 is sufficient in describing the temperature profile; only when both these conditions are violated do we need to resort to the full numerical solution of Eq. 4. These measurements indicate that in our main experiment (see the next section) we should expect the temperature rise outside the heater up to a few mK.

4 Main experimental setup

Our main experimental cell is a 3D-printed regular dodecahedron surrounding a spherical cavity ~ 16 mm in diameter that contains He II. A small spherical resistive heater ~ 1.8 mm in diameter is placed in the center, suspended by a cylindrical holder with a diameter of ~ 1 mm (see Fig. 3). On each of the remaining eleven flat outer surfaces, a circular hole is cut such that a circular second sound transducer

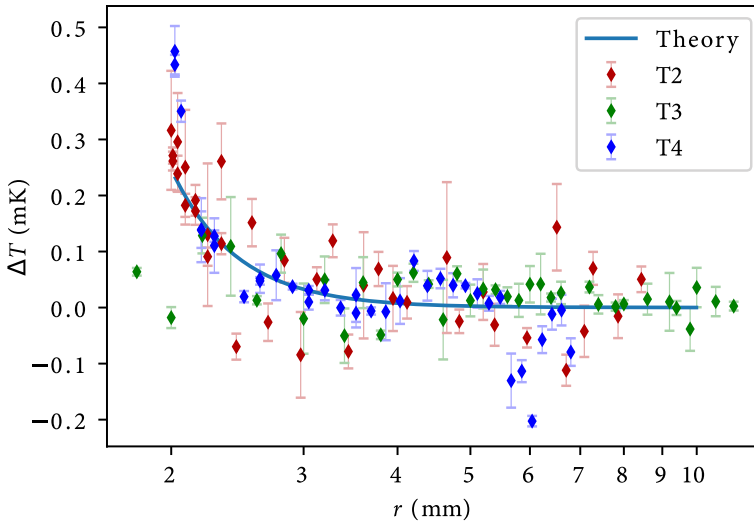


Fig. 2 The difference between the local temperature (measured using thermometers No 2, 3 and 4 shown in Fig. 1) and the bath temperature stabilized to $T = 1.5\text{K}$, plotted together with the numerically calculated temperature gradient (Eq. 4) versus the distance from center of the heater, powered by 500mW. The data points are highly scattered, likely due to noise; some of them might be rejected based on pending further analysis (Color figure online)

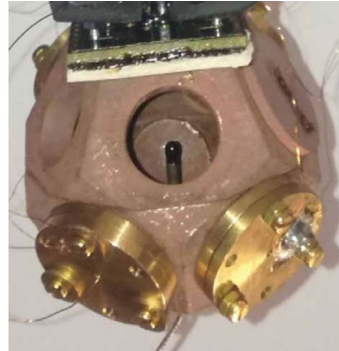
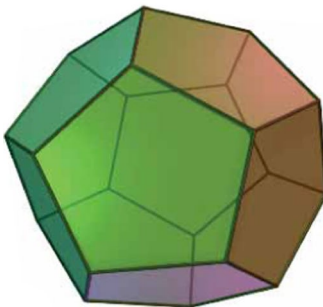


Fig. 3 Experimental cell is of the form of a regular dodecahedron outside (left) containing a nearly spherical sample of liquid helium inside. The photograph shows the cell with second sound transducers attached and the spherical heater in its center (Color figure online)

9 mm in diameter can be mounted in it. Each transducer consists of a brass cylinder connected to an electrode, with a thin micro-pore membrane attached on its inward face. The membrane is coated with a thin layer ($\sim 30\text{nm}$) of gold on the side facing away from the electrode. The second sound attenuation technique is described in detail in Refs. [15, 24].

The cell is affixed onto a cryogenic insert in a cylindrical helium bath (diameter $\sim 200\text{mm}$). The temperature of the bath is lowered and stabilized using a pumping

unit consisting of a Roots pump and a mechanical backing pump, with a PID regulation loop using a resistive heater for fine control. Vapour pressure of the bath is monitored by the MKS Baratron, and additional calibrated resistive thermometers [21–23] are installed at various locations inside the bath and measured by the Lake-Shore 336 temperature controller.

The heater is a small $\sim 50\ \Omega$ resistor encased in a Stycast 2850 sphere, as seen in the photograph in Fig. 3. It is driven by a DC voltage using a Keithley power supply and generates a nearly spherical counterflow. For the present experiment, we installed two second sound transducers diametrically opposing each other, one as the sound source driven by an AC signal from the Agilent 33220A function generator, the other as the second sound sensor monitored by the Stanford Research SR830 lock-in amplifier.

We performed measurements at various bath temperatures using different heater powers. At each temperature, with heater power off, we swept the frequency of the driving voltage on the second sound driver and measured the response from the sensor, locating the second sound resonance frequencies. Then, after fixing the drive at a chosen resonance frequency and the sensor being constantly monitored, we swept the heater power within a preset range, and the sensor signal amplitude was recorded as a function of power. We ensured that heater power stopped at each set value for sufficiently long time so that the temperature and vortex line density inside the cell had settled to steady-state distributions. Each amplitude A so measured can be compared to the amplitude without the heater A_0 and used to infer the vortex line density inside the cell.

To obtain the vortex line density L , we need accurate knowledge of the second sound waves inside the cell. Although similar experiments have been performed and analyzed in rectangular channels [15, 16, 24], we are still in the process of finalizing the numerical methods for the spherical geometry, therefore the detailed analysis will be available in a later paper. Meanwhile, however, we do have approximate solutions for second sound in a sphere.

5 Second sound in a spherical cell

Neglecting dissipative phenomena, the second sound wave can be described in terms of a scalar potential Φ , with the counterflow velocity given as $\mathbf{u}_{\text{ns}} = \nabla\Phi$. Assuming small temperature variations, Φ satisfies the standard wave equation $\nabla^2\Phi = c^{-2}\partial^2\Phi/\partial t^2$, where $c = c(T)$ is the second sound velocity. As our cell is spherical, we seek the radial modes of standing waves, thus

$$\frac{1}{r^2} \frac{\partial}{\partial r} \left(r^2 \frac{\partial \Phi}{\partial r} \right) = \frac{1}{c^2} \frac{\partial^2 \Phi}{\partial t^2}.$$

Separating variables, by letting $\Phi \equiv R(r)T(t)$, leads to

$$\frac{1}{Rr^2} \frac{\partial}{\partial r} \left(r^2 \frac{\partial R}{\partial r} \right) = \frac{1}{Tc^2} \frac{\partial^2 T}{\partial t^2} \equiv C \quad (6)$$

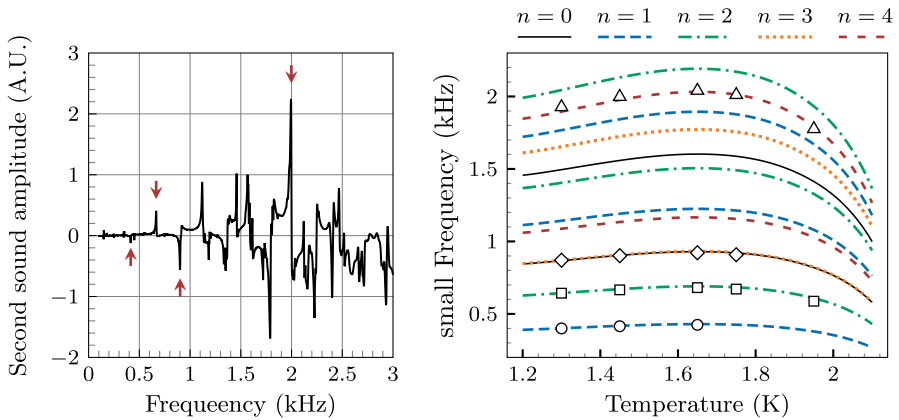


Fig. 4 Left: An example of the second sound sensor response to the frequency sweep with the heater off, at $T = 1.45$ K. The arrows mark the resonance frequencies chosen for subsequent attenuation measurements. Right: The second sound resonance frequencies calculated based on spherical Bessel functions plotted versus the temperature, in comparison with those measured. The legend denotes the order number, n , of the spherical Bessel function (Color figure online)

for some constant C . The eigen-solutions to the above equations are

$$R(r) = \alpha_n j_n(kr) + \beta_n y_n(kr), \tag{7}$$

$$T(t) = a \cos(ckt) + b \sin(ckt), \tag{8}$$

$$C = -k^2, \tag{9}$$

where j_n and y_n are the n th order spherical Bessel and Neumann functions, respectively. The equations are coupled through the wave vector k .

The solution domain is limited between two spherical surfaces, the inner one at the heater surface with radius r_0 , and the outer one at the cell wall with radius r_1 . A standing wave solution requires the sound amplitude to be zero at the boundaries, meaning $\partial R/\partial r = 0$ at $r = r_0$ and $r = r_1$. Therefore, for there to be a resonance at some wave vector k of mode n , there must exist values α_n and β_n such that

$$\alpha_n j'_n(kr_0) + \beta_n y'_n(kr_0) = 0, \quad \alpha_n j'_n(kr_1) + \beta_n y'_n(kr_1) = 0.$$

Here we used j' and y' to indicate spatial derivatives for brevity. For every given mode number n , multiple solutions for k can be obtained numerically. Each m th root of the n th mode, $k_{n,m}$, corresponds to a resonance frequency $f_{n,m} = ck_{n,m}/2\pi$. Note that solutions of k depend on geometry but not temperature. The frequency of the same resonance mode varies with temperature only through $c = c(T)$. In other words, all the curves in Fig. 4 have the same shape except for being scaled differently in the vertical direction.

This calculation enables us to compare the measured resonance frequencies against the theoretically predicted values. They match well, as shown in Fig. 4.

6 Conclusions

We have generated spherically symmetric thermal counterflow and verified the method of probing it by second sound attenuation inside a spherical cell surrounding a spherical heater placed in its center. Additionally, we have performed an accompanying experiment and directly measured the temperature gradient outside a spherical heater in open He II bath. The results of both experiments qualitatively confirm our model of thermal counterflow in spherical geometry. The ongoing detailed analysis should enable better knowledge of the vortex line distribution inside the cell and provide new insights into the generation, transportation and annihilation of quantized vortices in unbounded spherical thermal counterflow of He II.

The authors thank E. Varga for stimulating discussions and help at the early part of this project and acknowledge the support by the Czech Science Foundation under Project GAČR 20-00918S.

References

1. C.F. Barenghi, L. Skrbek, K.R. Sreenivasan, Introduction to quantum turbulence. *Proc. Natl. Acad. Sci. U.S.A.* **111**, 4649 (2014)
2. W.F. Vinen, Mutual friction in a heat current in liquid helium II, I. Experiments on steady heat currents. *Proc. R. Soc. A* **240**, 114 (1957)
3. W.F. Vinen, Mutual friction in a heat current in liquid helium II, II. Experiments on transient effects. *Proc. R. Soc. A* **240**, 128 (1957)
4. W.F. Vinen, Mutual friction in a heat current in liquid helium II, III. Theory of the mutual friction. *Proc. R. Soc. A* **242**, 493 (1957)
5. W.F. Vinen, Mutual friction in a heat current in liquid helium II, IV. Critical heat currents in wide channels. *Proc. R. Soc. A* **243**, 400 (1958)
6. J. T. Tough, *Superfluid turbulence*, in *Progress in Low Temperature Physics* (North-Holland Publ. Co., , Vol. VIII (1982)
7. A. Marakov, J. Gao, W. Guo, S.W. VanSciver, G.G. Ihas, D.N. Mc Kinsey, W.F. Vinen, Visualization of the normal-fluid turbulence in counterflowing superfluid He-4. *Phys. Rev. B* **91**, 094503 (2015)
8. J. Gao, E. Varga, W. Guo, W.F. Vinen, Energy spectrum of thermal counterflow turbulence in superfluid helium-4. *Phys. Rev. B* **96**, 094511 (2017)
9. R.J. Donnelly, *Quantized Vortices in Helium II* (Cambridge University Press, Cambridge, 1991)
10. L. Skrbek, D. Schmoranzler, Š Midlik, K.R. Sreenivasan, Phenomenology of quantum turbulence in superfluid helium. *Proc. Nat. Acad. Sci. USA* **118**, e2018406118 (2021)
11. E. Varga, Peculiarities of spherically symmetric counterflow. *J. Low Temp. Phys.* **196**, 28 (2019)
12. S. Inui, M. Tsubota, Spherically symmetric formation of localized vortex tangle around a heat source in superfluid ^4He . *Phys. Rev. B* **101**, 214511 (2020)
13. E. Rickinson, C.F. Barenghi, Y.A. Sergeev, A.W. Baggaley, Superfluid turbulence driven by cylindrically symmetric thermal counterflow. *Phys. Rev. B* **101**, 134519 (2020)
14. Y.A. Sergeev, C.F. Barenghi, Turbulent radial thermal counterflow in the framework of the HVBK model. *Europhys. Lett.* **128**, 26001 (2019)

15. E. Varga, M.J. Jackson, D. Schmoranzer, L. Skrbek, The use of second sound in investigations of quantum turbulence in He II. *J. Low Temp. Phys.* **197**, 130 (2019)
16. E. Varga, L. Skrbek, Thermal counterflow of superfluid He-4: temperature gradient in the bulk and in the vicinity of the heater. *Phys. Rev. B* **100**, 054518 (2019)
17. A. Sato, M. Maeda, and Y. Kamioka, in Proceedings of the Twentieth International Cryogenic Engineering Conference (ICEC20), edited by L. Zhang, L. Lin, and G. Chen (Elsevier Science, Oxford, 2005), Chap. 201, pp. 849-852
18. S.W. Van Sciver, *Helium Cryogenics* (Springer, New York, 2012)
19. J.D. Henberger, J.T. Tough, *Phys. Rev. B* **25**, 3123 (1982)
20. R.J. Donnelly, C.F. Barengi, *J. Phys. Chem. Ref. Data* **27**, 1217 (1998)
21. <http://microsensor.com.ua>
22. V.F. Mitin, P.C. McDonald, F. Pavese, N.S. Boltovets, V.V. Kholevchuk, IYu. Nemish, V.V. Basanets, V.K. Dugaev, P.V. Sorokin, R.V. Konakova, E.F. Venger, E.V. Mitin, *Cryogenics* **47**, 474 (2007)
23. V.F. Mitin, V.V. Kholevchuk, B.P. Kolodych, *Cryogenics* **51**, 68 (2011)
24. S. Babuin, M. Stammeier, E. Varga, M. Rotter, L. Skrbek, *Phys. Rev. B* **86**, 134515 (2012)

Publisher's Note Springer Nature remains neutral with regard to jurisdictional claims in published maps and institutional affiliations.